Removal of Toluene over NaX Zeolite Exchanged with Cu2+

Douglas Romero, Dayan Chlala, Madona Labaki, Sebastien Royer, Jean-Pierre Bellat, Igor Bezverkhyy, Jean-Marc Giraudon, Jean-Francois Lamonier

Catalysts **2015**, *5*, 1479-1497; doi:10.3390/catal5031479

OPEN ACCESS

catalysts

ISSN 2073-4344

www.mdpi.com/journal/catalysts

Article

Removal of Toluene over NaX Zeolite Exchanged with Cu^{2+}

Douglas Romero [1], Dayan Chlala [1,2], Madona Labaki [2], Sébastien Royer [3], Jean-Pierre Bellat [4], Igor Bezverkhyy [4], Jean-Marc Giraudon [1] and Jean-François Lamonier [1,*]

1 Unité de Catalyse et de Chimie du Solide UMR 8181 CNRS, Université Lille1 Sciences et Technologies, 59650 Villeneuve d'Ascq, France; E-Mails: douglas.romero@outlook.com (D.R.); dayane.chlela@univ-lille1.fr (D.C.); jean-marc.giraudon@univ-lille1.fr (J.-M.G.)

2 Laboratory of Physical Chemistry of Materials/PR2N, Faculty of Sciences, Lebanese University, Fanar, Lebanon; E-Mail: mlabaki@ul.edu.lb

3 Institut de Chimie des Milieux et Matériaux de Poitiers UMR 7285 CNRS, Université Poitiers, 86073 Poitiers, France; E-Mail: sebastien.royer@univ-poitiers.fr

4 Laboratoire Interdisciplinaire Carnot de Bourgogne UMR 6303 CNRS, Université Bourgogne, 21078 Dijon, France; E-Mails: jean-pierre.bellat@u-bourgogne.fr (J.-P.B.); igor.bezverkhyy@u-bourgogne.fr (I.B.)

***** Author to whom correspondence should be addressed; E-Mail: jean-francois.lamonier@univ-lille1.fr; Tel.: +33-3-2033-7733; Fax: +33-3-2043-6561.

Academic Editor: Keith Hohn

Received: 26 June 2015 / Accepted: 24 July 2015 / Published: 2 September 2015

Abstract: Toluene is a major air pollutant emitted from painting and metal coating processes and might have some health effects. Adsorption and catalytic complete oxidation are promising ways to retain or convert toluene into harmless products. The present work aims to develop a bifunctional material which can be used as an adsorbent and catalyst for low-temperature toluene removal. Copper zeolites were obtained by exchanging the sodium in the parent NaX zeolite with copper from aqueous solutions of $Cu(NO_3)_2{\cdot}2.5H_2O$. Several characterization techniques, H_2-TPR, XPS, XRD and N_2 physisorption, were used in order to evaluate the redox, surface, structural and textural properties of the materials, respectively. The various materials were tested in adsorption and catalytic processes. The sample with low copper content (1 wt. %) exhibited promising features in terms of toluene adsorption capacity and total oxidation. The results can be correlated to the presence of micropores and well-dispersed CuO species.

Keywords: VOC; toluene; catalytic oxidation; adsorption; zeolite; copper

1. Introduction

Volatile organic compounds (VOCs) are organic chemicals that have a high vapor pressure at room temperature. VOCs are numerous, varied and ubiquitous. Among them aromatic compounds are widely distributed in the environment and have been found to be a significant cancer risk factor, and to be implicated in neurological problems in urban children [1]. If inhaled or contacted, toluene can cause dermatitis (dry, red, cracked skin) and damage the nervous system and kidneys. Therefore, toluene emission control has become more stringent.

Natural sources of toluene are forest fires (incomplete combustion plants), volcanic eruptions and emissions from vegetation. These sources are minor compared with anthropogenic emissions from various oil conversion processes. Toluene emission results from the transformation of fossil fuels (oil, gas and coal). It is produced in combination with other substances (benzene, xylenes, *etc.*) as a result of various petrochemical processes such as catalytic reforming, steam cracking and dealkylation. Following petrochemical operations, the richest in toluene fractions will be distilled and purified to obtain pure trading toluene at 99%.

Toluene is a constituent of unleaded gasoline and replaced tetramethyl lead in order to improve the octane rating. As a result toluene is emitted during the vaporization of gasoline (petrol station, fuel transport and storage, *etc.*) and is present in vehicle exhaust gases (unburned products). Toluene is also found in industrial exhaust when used as a solvent or produced in the incineration processes.

Generally, the best way to reduce VOC emissions is to replace VOCs or to limit their use in industrial processes. If VOC substitution is not possible, it is necessary to control their emission in air using non-destructive or destructive methods [2]. The first group includes adsorption, absorption and condensation. Absorption and condensation are very useful in recovering expensive solvents and operating at a large capacity, but they require high capital and operating costs. Adsorption is a reliable alternative to eliminate organic compounds from industrial waste gases because of the flexibility of the system, low energy requirements and low operation costs [3]. The second group includes thermal and catalytic oxidation. Thermal oxidation, which requires high capital and operating costs, is the simplest method but it has to be carried out at high temperature, typically over 1000 °C. Also, this method can generate harmful by-products such as dioxin and nitrogen oxides [3].

In the case of toluene, control of its emission is often accomplished by catalytic oxidation or adsorption. Toluene removal by adsorption is the traditional method for cleaning air contaminants. However, the use of adsorbents just transfers pollutants from the gaseous phase to the solid phase and causes a disposal and regeneration problem. Catalytic oxidation is an attractive technique to selectively destroy this compound in CO_2 and H_2O. Catalytic oxidation of toluene can be carried out at temperatures 200–600 °C lower than that for thermal oxidation and has high selectivity for the formation of harmless reaction products such as H_2O and CO_2 [4]. Supported noble metal (Pt, Pd, Rh) materials have been intensively examined in VOC catalytic combustion, but their limited availability and high price have encouraged their replacement by other active phases [5–7]. Transition metal oxides

have been found to be very active and present advantages over noble metals associated with their lower cost, higher thermal stability and greater resistance to poisoning [8–10]. The most active and selective transition metal-containing catalysts for VOC total oxidation are based on copper oxides [11]. Usually, the active phase is supported on a porous material in order to expose their active phases in highly dispersed, easily reducible metal ions. Large pore zeolites are often chosen as supports because of their high specific surface area and acid-base properties, allowing high metal loading and generating specific interaction between the active phase and the support. In the literature, zeolites NaX and NaY have become of special interest in the oxidation of toluene, due to their large pore channel system and high specific surface area [12,13]. It has been shown that toluene adsorption performed on faujasites is appealing due to their incombustibility, great stability, hydrophobic character, and recovery at low temperature [14,15]. Benmaamar and Bengueddach [16] studied the capacity of NaY, KY, BaY, BaX and NaX zeolites to adsorb m-xylene and toluene-measuring adsorption isotherms at 298, 308, 318, and 333 K. The NaX and NaY zeolites presented the highest capacity for toluene and m-xylene adsorptions in comparison with the other samples.

For low pollutant concentrations in the atmosphere, VOC catalytic oxidation is unappealing due to high energy consumption. Conversely, the cost-saving adsorption-catalytic oxidation hybrid process is attractive. The adsorption process will first concentrate the VOC, followed by the catalytic process, by increasing the temperature. In this work, the performances of copper-exchanged X zeolites were studied, taking into consideration the individual adsorbent and catalytic properties of the solid in toluene adsorption and catalytic oxidation processes.

2. Results and Discussion

2.1. Characterization of the Materials

2.1.1. Redox Properties

H_2-TPR experiments were carried out to identify and to quantify the copper-species-exchanged zeolites and to characterize their reducibility. The reduction profiles of the copper-exchanged zeolite X samples as well as the one of NaX zeolites after calcination at 400 °C are presented in Figure 1. The reduction profiles for the copper-exchanged samples are characterized by two regions of hydrogen consumption: the low temperature region (LTR) from 200 to 520 °C, and the high temperature region (HTR) from 520 to 900 °C. The NaX sample does not show any reduction peaks in the studied temperature range. The CuX-B1 (see experimental Section 3.1) sample shows unresolved signals in the LTR and HTR regions, with less H_2 consumption in comparison to the other exchanged samples. The reduction profile shows two well-defined peaks in the LTR, with maxima at 300 and 380 °C and at 320 and 365 °C for CuX-B2 and CuX-B3 samples, respectively. In the HTR, one well-resolved peak can be observed, with the maximum at 620 °C for both samples. According to the literature [4,17,18], the reduction of Cu^{2+} ions occurs by one-step and two-step mechanisms. The reactions involved in the reduction process are the following [19]:

$$CuO + H_2 \rightarrow Cu^0 + H_2O \quad (1)$$

$$Cu^{2+} + 0.5H_2 \rightarrow Cu^{+} + H^{+} \quad (2)$$

$$Cu^{+} + 0.5H_2 \rightarrow Cu^{0} + H^{+} \quad (3)$$

The reduction of CuO aggregates takes place via a one-step mechanism (Equation (1)) and occurs in the low-temperature region, along with the reduction of Cu^{2+} to Cu^{+} (Equation (2)). Equation (3) corresponds to the reduction of the Cu^{+} formed during the previous reduction process. Torre-Abreu *et al.* [19] pointed out the presence of CuO species in copper-exchanged MFI and Y zeolites. The authors also reported two reduction peaks, the first one of greater area at 300 °C and the second in the range of 500–900 °C. This means that a significant fraction of the copper species in the solids goes through a one-step mechanism according to Equation (1), instead of a two-step mechanism. It is expected with copper exchange treatment that $[Cu(OH)]^{+}$ as well as $Cu(OH)_2$ species in solution are transformed into CuO, after the zeolite activation treatment, which is present within zeolite channels along with the exchanged Cu^{2+} ions [20,21].

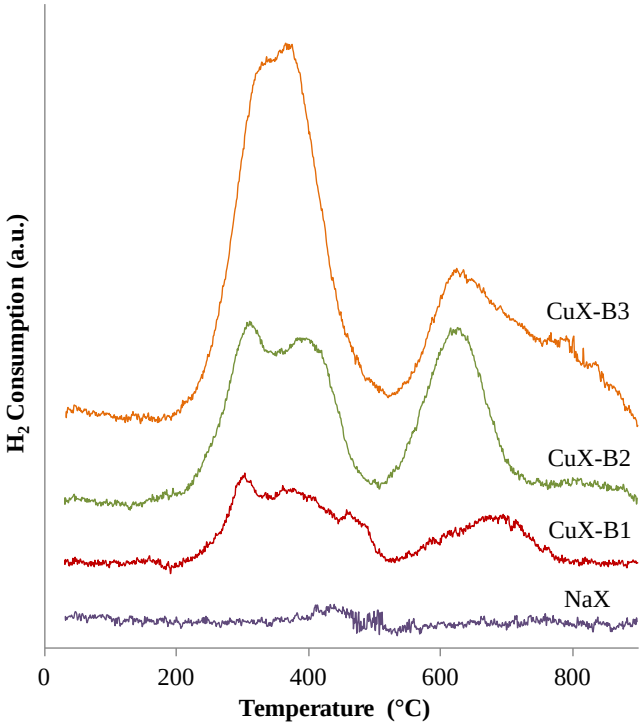

Figure 1. H_2-TPR profiles of the NaX and copper-exchanged zeolites.

Table 1 gathers the H_2 consumption values together with the theoretical copper content, calculated from the H_2 uptake and based in the stoichiometry of Equations (1) to (3). For the calculation, three assumptions are made:

(i) NaX sample is irreducible;
(ii) All the copper species are present as CuO and Cu^{2+} species in the copper-exchanged samples;
(iii) All the copper species are reduced by H_2 in the copper-exchanged samples into Cu^{0} species.

The copper content in the sample increases by repeated exchange treatments from CuX-B1 (1.1 wt. %) to CuX-B3 (4 wt. %). The difference in the H_2 consumption between the low-temperature

and high-temperature regions is an indication of CuO formation. The presence of the HT region peak for all samples indicates that a fraction of the copper + II is also present as Cu^{2+} ionic species. Table 1 gives the molar ratio between Cu^{2+} ions and total copper in the sample, calculated from the H_2 uptake of the LT and HT peaks. Whatever the copper content, this ratio is close to 0.6–0.7. It follows that the fraction of CuO species is rather similar in the three materials. The degree of exchange (in %) has been estimated from this ratio and the degree increases with the copper content in the zeolite (Table 1).

Table 1. Quantitative results from H_2-TPR experiments for NaX and copper-exchanged zeolites.

Sample	Consumed H_2 (mmol/g)	LTR Consumed H_2 (mmol/g)	HTR Consumed H_2 (mmol/g)	Copper Content (wt. %) *	Molar Ratio Cu^{2+}/Cu_{total}	Degree of Exchange
NaX	0.02	-	-	-	-	-
CuX-B1	0.17	0.12	0.05	1.1	0.6	2.0
CuX-B2	0.36	0.23	0.13	2.3	0.7	5.3
CuX-B3	0.62	0.41	0.21	4.0	0.7	8.5

***** Calculated from the H_2 uptake.

2.1.2. Bulk Structure

The wide angle power XRD patterns of the copper-exchanged zeolite X samples as well as the parent one (NaX) after calcination at 400 °C are displayed in Figure 2. The diffractrogram of the NaX sample shows the characteristic peaks of the crystalline faujasite framework ($Na_{88}Al_{88}Si_{104}O_{384}(H_2O)_{220}$ JCPDS 01-070-2168) [22,23]. The XRD patterns of the CuX-B materials are similar to that of pure NaX. No shift in the peak positions and no new phase have been observed for CuX-B samples. This result suggests that the copper species are probably well dispersed in the zeolite structure. A decrease in the intensities of the diffraction peaks can be also observed, indicating a certain loss of crystallinity.

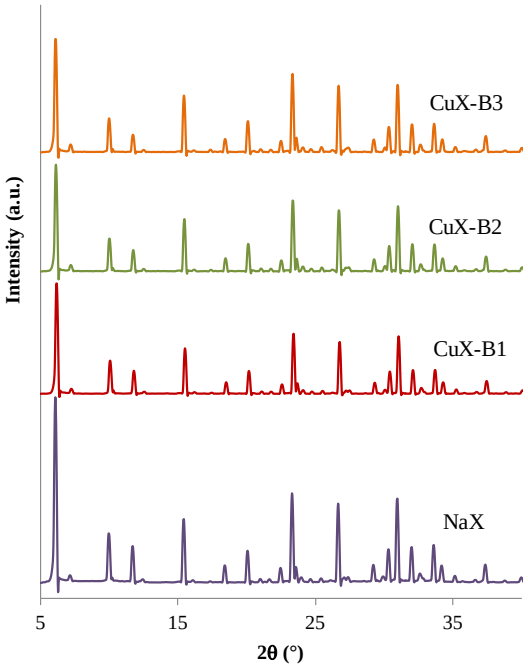

Figure 2. XRD patterns of the NaX and copper-exchanged zeolites.

Abu-Zied [22] obtained similar results in samples prepared by exchanging a NaX zeolite with different concentration of aqueous copper(II) acetate solutions. Benaliouche *et al.* [23] also observed no shift in the peak positions and no significant diffraction lines assigned to any new phase in Ag^{+}- and Cu^{2+}-exchanged X zeolites prepared from $AgNO_3$ or $CuCl_2$ aqueous solutions. The authors concluded from these results, that both Ag^{+} and Cu^{2+} seemed to be well dispersed in the zeolite framework.

2.1.3. Specific Surface Area

N_2 physisorption isotherms obtained for the samples after calcination at 400 °C are presented in Figure 3. The isotherms of the samples show a type I in Brunauer, Deming, Deming and Teller (BDDT) classification [24], which is typical of microporous materials. Upon copper treatment, the adsorption capacity decreases with the increase in Cu-exchange and a hysteresis loop appeared on the CuX-B2 and CuX-B3 samples, suggesting that ink-bottle type mesopores are formed on these zeolites [22]. According to the shapes of the isotherms the filling of micropores is done for approximately P/P_0 = 0.2; beyond that point, adsorption takes place outside micropores. The adsorbed quantity between P/P_0 = 0.2 and 0.95 is usually quite small, around 4% to 6% compared to that adsorbed inside the micropores.

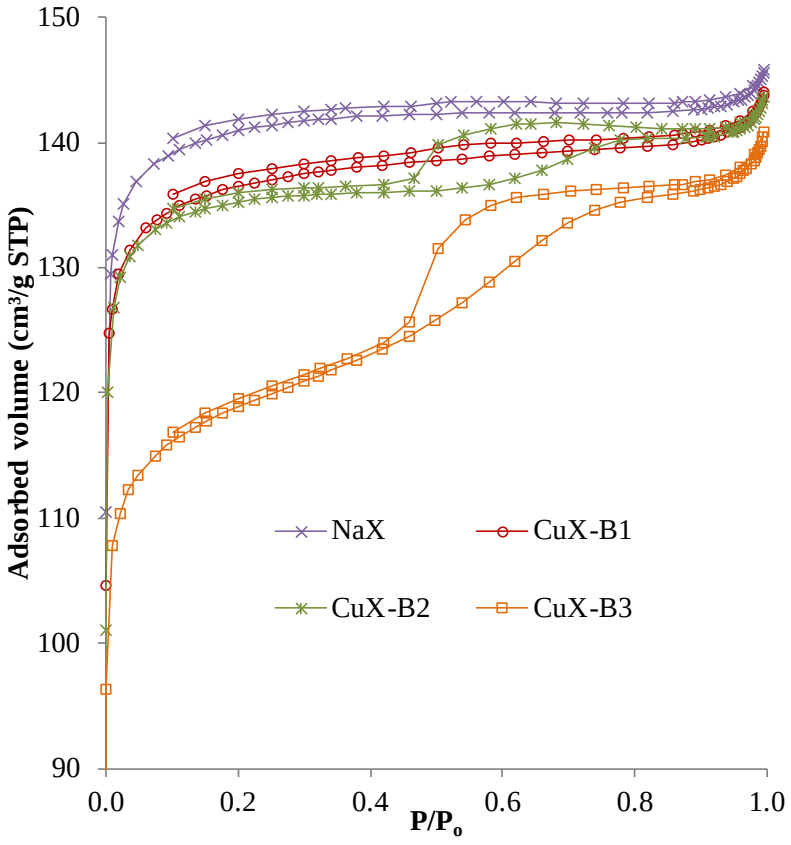

Figure 3. Adsorption-desorption isotherms of the NaX and copper-exchanged zeolites.

The textural properties of the samples are listed in Table 2. The NaX sample presents a specific surface area of 451 m^2/g, which is in the order of the values reported in the literature for this type of zeolite [22,25,26]. However, Cu addition leads to a decrease in the specific surface area of the copper-exchanged samples, the effect being more important for the CuX-B3 sample, which is

the sample with the highest degree of exchange (see Table 1). Benaliouche *et al.* [23] also observed a decrease in the specific surface area in Ag^{+} and Cu^{2+} exchanged X zeolites prepared from $AgNO_3$ or $CuCl_2$ aqueous solutions, and attributed this behavior to the partial blocking of the zeolite pore access by Ag and Cu ions, leading to a reduction in total specific surface area. The exchange treatment do not cause a significant effect on the pore volume of the samples, since a slight decrease is observed in comparison to the NaX zeolite. However, considering the micropore volume (Table 2), the decrease is more pronounced and seems to be correlated to the increase of copper content in the sample. For NaX material, the micropore volume represents 97% of pore volume, whereas the value drops to 85% for the CuX-B3 sample.

Table 2. Textural properties of the NaX and copper-exchanged zeolites.

Sample	Specific Surface Area (m^2/g)	Pore Volume * (cm^3/g)	Micropore Volume ** (cm^3/g)
NaX	451	0.226	0.218
CuX-B1	434	0.223	0.211
CuX-B2	432	0.222	0.201
CuX-B3	384	0.218	0.185

***** Calculated at $P/P_0 = 0.98$; ****** Calculated from the equation proposed by Dubinin [24].

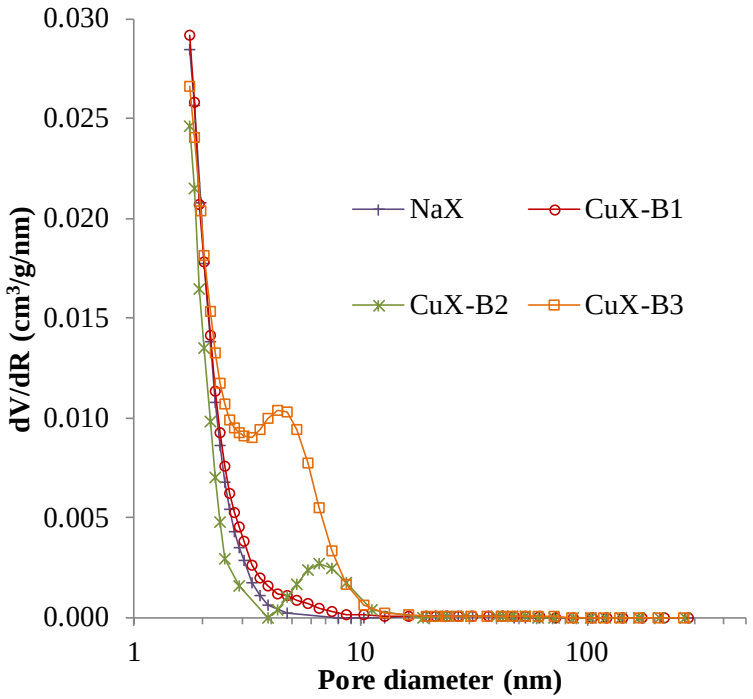

Figure 4. Pore size distribution of the CuX-B materials and the parent NaX zeolite.

Figure 4 shows the pore size distribution of the samples. Exchanging the NaX zeolite with solutions of copper results in emergence of a peak in the mesoporous region, centered at 6.5 and 4.5 nm for the CuX-B2 and CuX-B3 samples, respectively. Abu-Zied [22] obtained this behavior for Cu^{2+}-acetate exchanged X zeolites. The author observed two peaks at 3.9 and 6.5 nm and 3.9 and 4.9 nm for the lowest copper content catalysts, 2.6 and 7.3 wt. %, respectively. Hammoudi *et al.* [26] reported a decrease in the N_2 uptake with an increasing number of Cu^{2+} ions in copper-exchanged X zeolites; the authors suggested that the zeolite could endure a structural deformation at higher levels of

exchange, that would consist in a modification of the supercage geometry which would impact the adsorption characteristics of the parent zeolite, in terms of the interaction of the adsorbate molecules with the zeolite surface through lattice oxygen atoms and accessible extraframework cations. However, in our case, the degree of Na^+ exchange is not so high (less than 9%) (Table 1). Therefore, in the case of CuX-B2 and CuX-B3 samples, the increase in copper content could explain this additional mesoporosity arising from the CuO species which are less dispersed and could contribute to the porosity at 6.5 and 4.5 nm.

2.1.4. XPS Analyses

The XPS spectra of the core levels of the Cu 2p were analyzed to estimate the copper oxidation state. The samples show two peaks in Figure 5, which intensity increase with copper content; the binding energy (BE) of the first one is centered at 934.6–934.9 eV (Cu $2p_{3/2}$) (Table 3) whereas the BE of the second one is at 954.3 eV (Cu $2p_{1/2}$). The presence of a shake-up satellite is also observed at around 944.5 eV, especially for the CuX-B3 sample (Table 3 and Figure 5). The presence of this shake-up satellite peak is characteristic of the presence Cu(II) species [27]. Ning *et al.* [28] reported Cu $2p_{3/2}$ peaks centered at 934.7 eV in samples of Na-ZSM-5 exchanged with copper, which were assigned to the presence of CuO. They also reported other Cu $2p_{3/2}$ peaks centered at 932.52 eV related to Cu_2O. It is worth noting that the Cu $2p_{3/2}$ photopeak BE observed for the materials are located at higher BE than those reported in the literature for bulk copper materials. For example, Morales *et al.* [29] reported that Cu $2p_{3/2}$ BE in CuO is 933.7 eV. The highest BE value of electrons coming from the 2p level of Cu in zeolites in comparison to those in bulk metal oxides has been already reported [30,31]. The shifts reflected the presence of small clusters of ions together with isolated metal ions dispersed in the zeolite [27]. Then, the values of 934.6–934.9 eV for BE Cu $2p_{3/2}$ are in line with the presence of Cu^{2+} ions and CuO species suggested by TPR analyses.

Table 3. Surface composition (at. %) of the NaX and copper-exchanged zeolites, Cu $2p_{3/2}$ BE (eV) and satellite (Sat) Cu $2p_{3/2}$ BE (eV) in the copper-exchanged zeolites.

Sample	Si (at. %)	Al (at. %)	O (at. %)	Na (at. %)	Cu (at. %)	Cu $2p_{3/2}$ (eV)	Sat Cu $2p_{3/2}$ (eV)
NaX	13.4	9.6	61.4	15.6	-	-	-
CuX-B1	14.3	10.8	61.6	12.5	0.8	934.9	944.5
CuX-B2	15.1	10.7	63.9	9.2	1.1	934.6	944.3
CuX-B3	15.0	12.0	63.3	8.0	1.7	934.6	944.7

Figure 6 shows the Na 1s and O 1s core level spectra of the different samples. Figure 6a shows that the Na 1s photopeak decreases in intensity from the parent zeolite (NaX) to the Cu^{2+} exchanged samples, a result that supports the behavior observed in the Cu 2p photopeak. Quantitative results corroborate this trend (Table 3). Interestingly, Na 1s BE is shifted to lower value with copper addition, showing an evidence of change in Na species surrounding. A decrease in O 1s intensity and a change in the O 1s shape are clearly observed from NaX to CuX-B3 materials (Figure 6b). Almeida *et al.* [32] reported that the O 1s peak in the NaX zeolite originates from oxygen atoms belonging to different environments: aluminate anions compensated by sodium cations, NaAlO, SiOSi bonds and silanol groups, SiOH. They determined that the contribution from the NaAlO signals decreased in zeolites exchanged with Cs and

ammonium ions in comparison to the original NaX zeolite. Therefore, the change in the shape of the O 1s peak could be interpreted as a decrease in the contribution of NaAlO component resulting from Na^{+}–Cu^{2+} exchange.

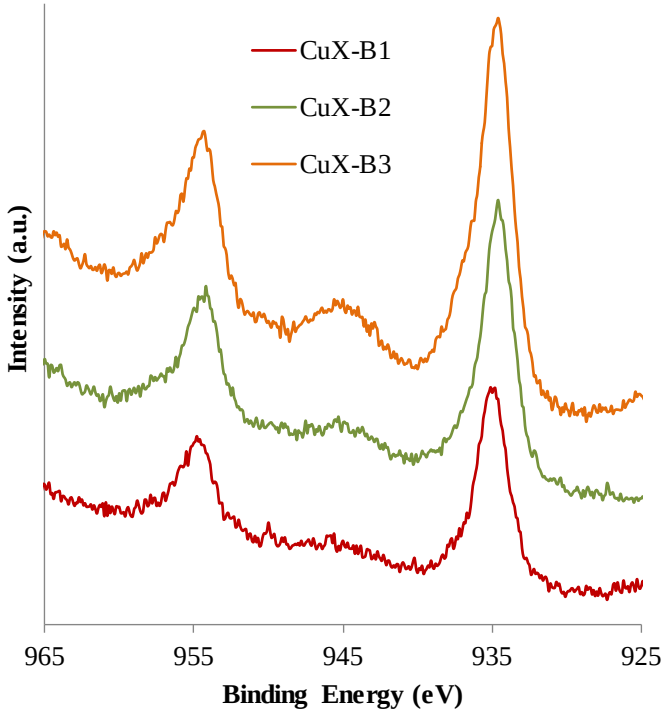

Figure 5. Cu 2p XPS spectra of the copper-exchanged zeolites.

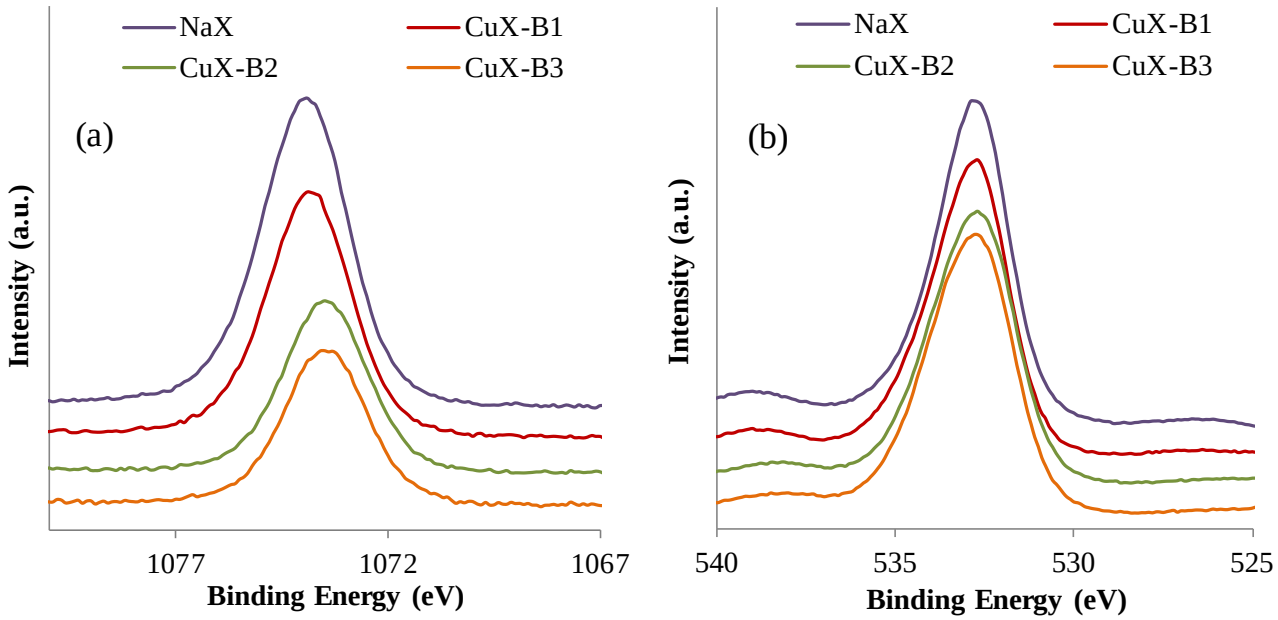

Figure 6. (**a**) Na 1s and (**b**) O 1s XPS spectra of the NaX and copper-exchanged zeolites.

2.2. Adsorption Tests

Figure 7 shows the toluene adsorption breakthrough curves of the NaX and copper-exchanged zeolites depicted by the variation in the C/Co ratio *vs* the test duration, where Co and C are the inlet and outlet

concentrations, respectively. All the breakthrough curves reach adsorption equilibrium, but the samples exhibit different behaviors. Table 4 presents the parameters associated with the behavior of the samples in relation with their properties for toluene adsorption.

Among the samples, CuX-B1 shows the higher adsorption capacity and the longest breakthrough time compared with the other materials, reaching 22.2 g toluene/100 g solid and 473 min, respectively. This result for adsorption capacity is in the order of the values that can be found in the literature for other materials. For example it has been reported for activated carbon values between 11 and 34 g toluene/100 g solid [33]. All other samples exhibit a similar breakthrough time at about 260 min but differ in the time needed to reach the saturation point. The samples can be ranked by their ease in reaching adsorption equilibrium: NaX < CuX-B1 < CuX-B2 < CuX-B3, and by their decreasing adsorption capacity: CuX-B1 > NaX > CuX-B2 > CuX-B3 (Figure 7). On the other side, the NaX presents the highest PUB (percentage of unused bed) value, which can be related to the fact that the residence time of toluene molecules in the bed is not enough to benefit from all the extension of the NaX bed.

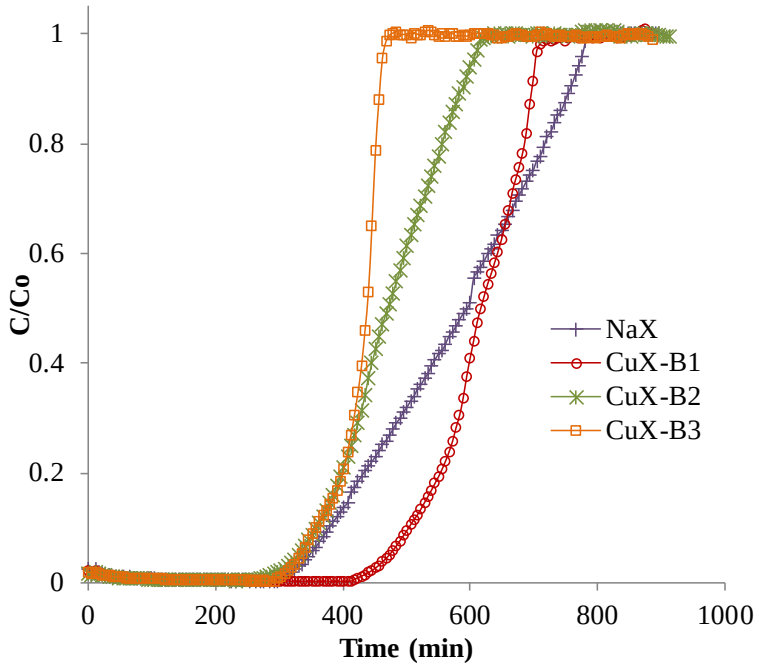

Figure 7. Adsorption breakthrough curves of toluene over NaX and copper-exchanged zeolites.

The difference between samples could be attributed not only to a difference in the copper content, but also to the difference in their textural properties. Archipov *et al.* [34] studied the adsorption of benzene in copper-exchanged Y zeolites, using Fourier transform infrared spectroscopy; the authors found that benzene adsorbed on both copper and brønsted acid sites of the zeolite, but preferentially on copper site. With the assumptions of a similar behavior for the toluene-zeolite system, it can be expected that the copper-exchanged samples exhibit higher capacities of adsorption in comparison to the NaX zeolite. However CuX-B2 and CuX-B3 samples show less capacity for adsorption. These results may be explained by a decrease in the specific surface area affecting mostly the micropore volume (Table 2). It has been pointed out in the literature that the micropore volume of an adsorbent plays an important role in the adsorption of toluene. Zhang *et al.* [35] reported for several types of adsorbents, such as SBA-15, MCM-41, NaY and SiO_2, that the volume of micropores was an important parameter for the adsorption

of VOCs. It was found that the amount of adsorbed toluene was linearly correlated to the micropore volume and that the presence of micropores directly led to an increase in the dynamic adsorption capacity of VOCs. Lillo-Ródenas *et al.* [33] also obtained such a correlation between the capacity of toluene and benzene adsorptions for different types of activated carbon and the total volume of micropores.

Table 4. Adsorption parameters of the NaX and copper-exchanged zeolites.

Sample	Adsorption Capacity (g/100 g Solid)	*t* 5% (min)	*t* 50% (min)	*t* 95% (min)	PUB (%)
NaX	20.1	347	594	770	40
CuX-B1	22.2	473	616	704	23
CuX-B2	16.7	330	473	605	31
CuX-B3	15.1	336	440	462	21

2.3. Catalytic Tests

Figure 8 shows the catalytic performances of the three copper-exchanged zeolites and the parent zeolite NaX, in terms of toluene conversion as a function of temperature. The toluene concentration reaches the maximum value (conversion = 0) at 50 °C. After this point, the concentration decreased progressively as the conversion increased, reaching the minimum value (conversion = 98%) at around 263, 320 and 346 °C ($T_{98\%}$) for CuX-B1, CuX-B2 and CuX-B3, respectively (Table 5).

Considering the $T_{50\%}$ as a measure of the catalytic performances of the materials, the activity order can be established as CuX-B1 > CuX-B2 > CuX-B3 > NaX. A remarkable improvement can be observed in the catalytic performance after the copper exchange treatment of the parent zeolite. Among the copper-exchanged samples, CuX-B1 presents the best catalytic performance, even though the copper loading in the sample is the lowest. By contrast, in the literature an increase in the toluene conversion has been reported with the copper content increase in the zeolites. For example, Antunes *et al.* [4] reported that the oxidation of toluene is dependent on the copper content and the degree of copper exchange in the NaHY zeolite. A very low CuO quantity has been observed in the samples and the sample with the lowest copper content (1.1%) was classified as quasi-inactive for toluene oxidation. A similar result was obtained by Ribeiro *et al.* [13], who studied the evolution of $T_{50\%}$ as a function of the Cu loading from 0 to 5 wt. % for series of CuHY and CuCsHY zeolites, and showed a decrease of the light-off temperatures when copper content of the catalysts is increasing. It has also been reported [20] for Cu ions exchanged in ZSM-5 zeolites that well dispersed CuO species exhibited higher oxidation activity and reducibility in comparison with the exchanged Cu ions. In comparison with literature data [4] and in similar experimental conditions, our copper-exchanged zeolites are much more active in the toluene oxidation. Therefore we suggest that a high copper content and high Na^+ exchange is not required for toluene oxidation. Well dispersed CuO are most probably the active species which are easily reducible by the toluene molecule (redox mechanism). Increasing the copper content in the sample led to the decrease in CuO species dispersion, species less accessible and less active for toluene oxidation (Figure 8).

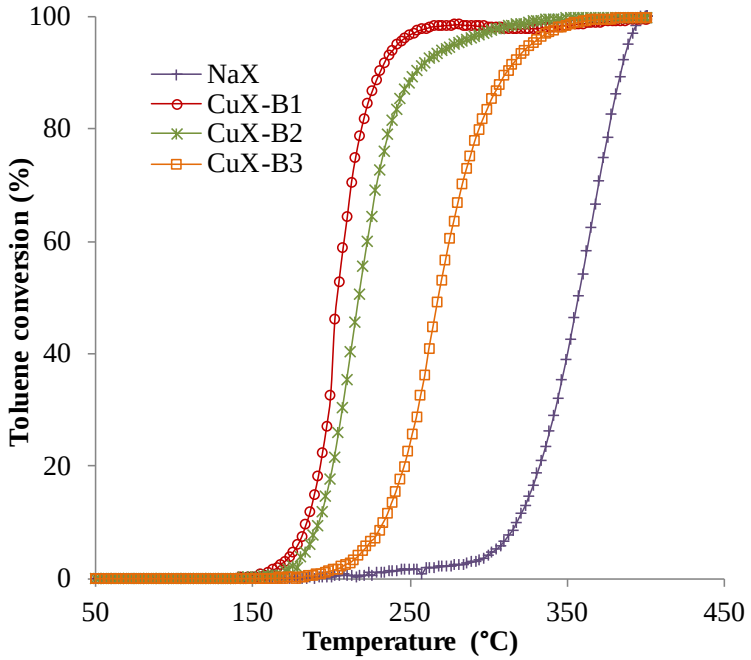

Figure 8. Toluene conversion as a function of the temperature reaction in the presence of different catalysts.

Table 5. Catalytic performances of the NaX and copper-exchanged zeolites.

Sample	$T_{50\%}$ (°C)	$T_{98\%}$ (°C)
NaX	357	394
CuX-B1	203	263
CuX-B2	217	320
CuX-B3	270	346

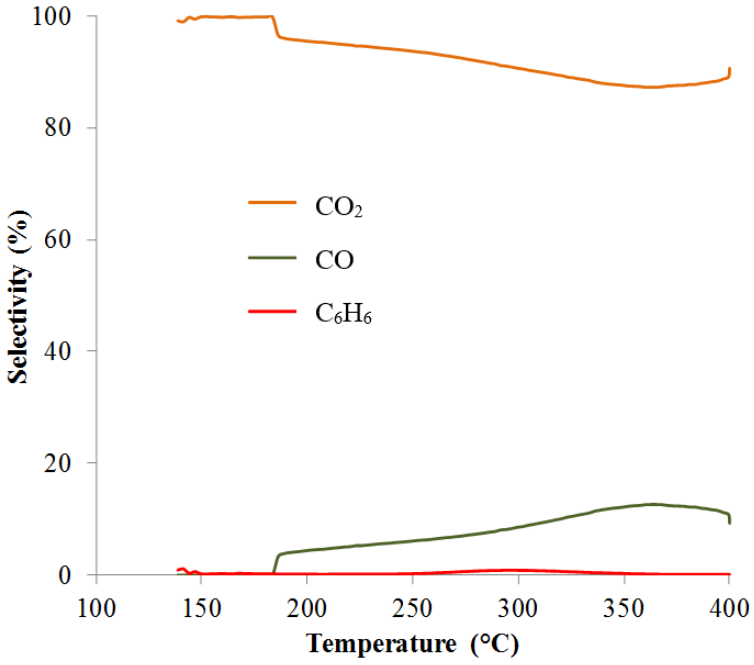

Figure 9. Variation of CO_2, CO and benzene selectivities (%) with the reaction temperature over CuX-B1 catalyst.

Boikov *et al.* [36] proposed a mechanism for the selective catalytic oxidation of toluene using V_2O_5 and MoO_3 as catalysts. According to the mechanism, toluene is first oxidized to benzene, through the formation of benzaldehyde as an intermediate. Then, benzene is oxidized to benzoquinone to yield carbon oxides. Figure 9 shows the variation of the selectivities in CO_2, CO and benzene during the catalytic test for the CuX-B1 catalyst. CuX-B2 and CuX-B3 samples presented similar results. At 400 °C, the selectivity towards CO_2 is 90.6%, whereas the selectivity in CO is 9.7%. No benzene is detected, evidencing the high performances of copper-exchanged zeolites in the oxidation of gaseous toluene reactant in carbon monoxide, carbon dioxide and water products.

3. Experimental Section

3.1. Materials Synthesis

CuX materials were synthesized by an ion exchange using a commercial NaX zeolite (Si/Al = 1.3). The zeolite NaX was exchanged with aqueous solutions of $Cu(NO_3)_2{\cdot}2.5H_2O$ (99.99% metal basis, Sigma-Aldrich, St. Louis, MO, USA, as received). 7 g of parent zeolite were stirred at room temperature in 350 mL of aqueous solution containing 5×10^{-3} mol/L of the metal nitrate for 24 h. The sample was filtered, washed thoroughly and dried overnight at 373 K. This material was called CuX-B1. Higher degrees of copper exchange in the zeolite were obtained by repeated treatments. CuX-B2 was obtained by stirring 4 g of the CuX-B1 material with 200 mL of the solution for the same time and applying the same procedure. Finally, CuX-B3 was synthesized from CuX-B2 material, stirring 2 g of the solid with 100 mL of the solution [37,38]. The copper-exchanged level extent was evaluated assuming that one Cu^{2+} ion can replaced two Na^+ ions in the zeolite.

3.2. Characterization Techniques

Powder X-ray diffraction (XRD) patterns were recorded on a Bruker D8 X-ray diffractometer (Champs-sur-Marne, France) at room temperature with CuKα radiation (λ = 1.5418 Å). The diffractograms were recorded for 2θ values comprised between 5° and 80° using a 0.04° step with an integration time of 2 s. The diffraction patterns were indexed by comparison with the Joint Committee on Powder Diffraction Standards files (JCPDS).

XPS experiments were performed using an AXIS Ultra DLD Kratos spectrometer (Manchester, UK) equipped with a monochromatised aluminum source (Al Kα = 1486.69 eV) and charge compensation gun. All binding energies were referenced to the C 1s core level at 285 eV. Simulation of the experimental photopeaks was carried out using a mixed Gaussian/Lorentzian peak fit procedure by means of the CasaXPS software.

Temperature programmed reduction (H_2-TPR) measurements were performed on a Micromeritics AutoChem apparatus (Verneuil en Halatte, France). H_2-TPR was performed in a quartz microreactor (9 mm). The H_2-TPR was conducted in two stages:

1. Degassing treatment to remove the adsorbed species: The sample was heated from room temperature to 200 °C (10 °C/min) under an argon flow (50 mL/min). The sample was then maintained at 200 °C for 1 h and cooled to room temperature under argon atmosphere.

2. Reduction process: The reduction mixture containing 5% *v*/*v* H_2 in argon was send to the sample at room temperature, the flow was 50 mL/min. After a short stabilization process the temperature was increased from room temperature to 900 °C (with 10 °C/min heating rate). Finally, the sample was cooled to room temperature under argon.

N_2 adsorption-desorption isotherms were recorded at −196 °C using an automated ASAP2010 and TRISTAR II apparatus from Micromeritics. Before the adsorption-desorption experiment, the sample was heated at 120 °C under vacuum for 3 h for degassing and the adsorbed species was removed. Specific surface areas were calculated from the linear part of the Brunauer-Emmett-Teller line whereas the micropore volumes were calculated from the Dubinin method commonly used for adsorption description in microporous materials [24]. The desorption branch of the isotherm was used for the evaluation of the pore size distribution.

3.3. Toluene Catalytic Oxidation Test

The catalytic activity of materials for toluene oxidation is typically compared using light off curves, curve of conversion *versus* reaction temperature, where the reactant mixture passes through a catalyst bed while the temperature is increased [26]. The subsequent S-shaped curves give an idea of the performance of different catalysts as well as total conversion minimal temperature. The toluene catalytic setup is presented in Figure 10.

The gaseous toluene was generated using a saturator containing reagent-grade toluene in liquid phase. The saturator is a small and inert capsule containing a pure chemical compound in two phases between its gas and liquid phases. The release of the chemical occurs when a carrier gas (in this case air) passes through the device and reaches a saturated state. The temperature controller of the thermostatic bath maintains the saturator temperature at a set point of 65 °C with an accuracy of 0.01 °C. This gives a toluene concentration in the air stream of 800 ppm.

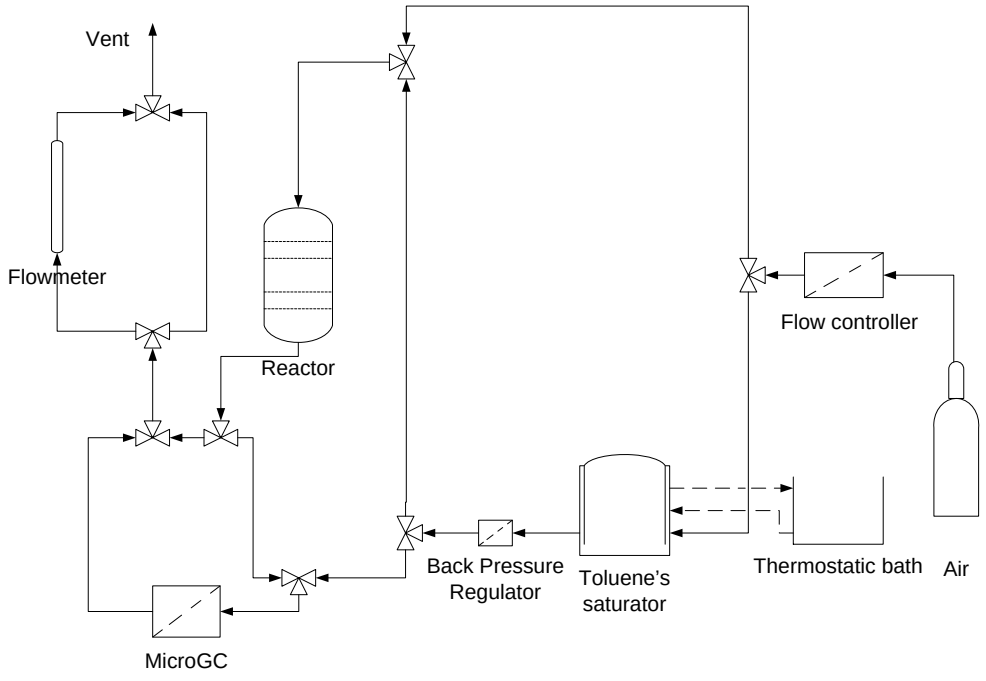

Figure 10. Toluene adsorption and catalytic setup.

Toluene complete catalytic oxidation produces only CO_2 and H_2O. However, incomplete oxidation products can be obtained, such as CO and benzene, among others. Analysis of these compounds was performed using a microGC from SRA Instruments (Marcy l'Etoile, France). Quantification was realized by calibration of peak areas, and for each compound, linear regression was used to determine the response factors.

The toluene conversion was estimated using the following equation:

$$X_{\text{toluene}}(\%) = \left(1 - \frac{[\text{toluene}]}{[\text{toluene}] + [\text{benzene}] + [\text{CO}] + [\text{CO}_2]}\right) \times 100 \quad (4)$$

The selectivity towards products was estimated with the following equation, which was written for the specific case of CO:

$$S_{\text{CO}}(\%) = \left(\frac{[\text{CO}]}{[\text{toluene}] + [\text{benzene}] + [\text{CO}] + [\text{CO}_2]}\right) \times 100 \quad (5)$$

The toluene catalytic oxidation was performed in a fixed bed reactor (i.d. 8–10 mm). In a test, 200 mg of the catalyst was loaded in the reactor. The total flow rate was 100 mL/min and the gas hourly space velocity was 30,000 mL/gcat.

- Step 1: Catalyst activation is the first step of the catalyst test. The conditions employed are an air stream with a flow of 70 mL/min. The aim of this activation process is to clean the catalyst surface and remove physisorbed water and surface impurities that can eventually be present on the catalyst.
- Step 2: The toluene catalytic oxidation start, the temperature is increased and the effluent gas from the reactor is analyzed using an on-line microGC analyzer; injections were made every five minutes.

3.4. Toluene Adsorption Test

The adsorption capacity of the samples was measured employing the same system depicted in Figure 10 and measuring the variation of the ratio of outlet (C) and inlet (Co) concentrations with time. The results are typical S-shape curves. The first toluene adsorption is nearly complete and the breakthrough curves are adjacent to a straight line. In the second, the concentration of the toluene slowly reaches the breakthrough point and the outlet toluene concentration increased with the extension of adsorption time. At this end the outlet concentration rise to the inlet concentration [35]. For a given concentration, the longer breakthrough and saturation time means a greater adsorption capacity. The adsorption capacity (AC) was calculated by the numerical integration of the breakthrough curve, using the following equation:

$$\text{AC} = \frac{\text{Area} \times C_0}{W_s} \quad (6)$$

where:

$\text{Area} = \int_{t0}^{tf} C / C_0 \mathrm{d}t$, C_0 = Initial concentration, W_s = Sample weight.

The times at which the outlet toluene concentration was 5% (t 5% = breakpoint time), 50% (t 50% = stoichiometric time) and 95% (t 95% = saturation time) of the inlet toluene concentration were also estimated. The percentage of unused bed (PUB) was calculated from the length of unused bed (LUB) by using the following equations:

$$\mathrm{LUB} = L\left(1 - \frac{\mathrm{AC}_{t5\%}}{\mathrm{AC}_{t95\%}}\right) \text{ and } \mathrm{PUB}(\%) = \frac{\mathrm{LUB}}{L} \times 100 \quad (7)$$

where: L = total length of the bed, $\mathrm{AC}_{t\ 5\%}$ and $\mathrm{AC}_{t\ 95\%}$ = adsorption capacity at t 5% and t 95% respectively.

The toluene's concentration, flow of stream and mass of the adsorbent were empirically adjusted in order to have acceptable adsorption times before the breakpoint for comparison purposes between samples. The temperature of the thermostatic bath was maintained at 25 °C, the mass of the sample loaded in the reactor was 200 g and the total flow rate was 13 mL/min. This gives a toluene concentration in the air stream of approximately 1250 ppm. For the adsorption test, activated samples (400 °C with an air flow of 70 mL/min) were exposed to the toluene stream at a temperature of 30 °C. The effluent gas from the reactor was analyzed using on-line microGC analyzer; injections were made every five minutes.

4. Conclusions

In this study the potential of copper-exchanged zeolites as a toluene adsorbent and as a catalyst for toluene total oxidation was evaluated. A low quantity of copper (from 1 wt. % to 4 wt. %) was deposited into the zeolite as copper + II species. Through the consequent exchange, it has been shown that the fraction of copper-exchanged (Cu^{2+} species) *versus* CuO species remained rather constant whatever the copper content. The toluene adsorption studies have shown that when the microporosity is maintained for low-copper-content zeolite, the adsorption capacity of the corresponding material (CuX-B1) is not affected in comparison with the parent zeolite. Interestingly, this material exhibited remarkable toluene oxidation due to the presence of well-dispersed CuO species.

The individual adsorbent and catalytic properties of CuX-B1 sample are promising, and this material can be considered a potential hybrid system for the treatment of toluene in low concentrations in air.

Acknowledgments

The Chevreul institute (FR 2638), Ministère de l'Enseignement Supérieur et de la Recherche, Région Nord–Pas de Calais and FEDER are acknowledged for supporting and funding this work. The French Agency for Sustainable Development, ADEME, is also acknowledged for its financial support through CORTEA program n°11-81-C0108. This work was also supported by a grant from the project PHC CEDRE 2015 N° 32933QE. D. C. acknowledges the award of a doctoral fellowship from the Agence Universitaire de la Francophonie (AUF)—Région du Moyen-Orient.

Author Contributions

D.R. and D.C. performed the experiments and analyzed the data; M.L. and S.R. contributed to the interpretation of the materials characterization results. J.P.B. and I.B. contributed towards the interpretation of the adsorption tests results. J.M.G. and. J.F.L. contributed towards the interpretation of the catalytic results. D.R., J.M.G. and J.F.L. contributed to the writing of the manuscript.

Conflicts of Interest

The authors declare no conflict of interest.

References

1. Kostiainen, R. Volatile organic compounds in the indoor air of normal and sick houses. *Atmos. Environ.* **1995**, *29*, 693–702.
2. Soylu, G.; Özcelik, Z.; Boz, I. Total oxidation of toluene over metal oxides supported on a natural clinoptilolite-type zeolite. *Chem. Eng. J.* **2010**, *162*, 380–387.
3. Kima, H.; Kimb, T.; Koh, H.; Lee, S.; Mina, B. Complete benzene oxidation over Pt-Pd bimetal catalyst supported on γ-alumina: Influence of Pt-Pd ratio on the catalytic activity. *Appl. Catal. A* **2005**, *280*, 125–131.
4. Antunes, A.; Ribeiro, M.; Silva, J.; Ribeiro, F.; Magnoux, P.; Guisnet, M. Catalytic oxidation of toluene over CuNaHY zeolites, Coke formation and removal. *Appl. Catal. B* **2001**, *33*, 149–164.
5. Tidahy, H.; Siffert, S.; Wyrwalski, F.; Lamonier, J.-F.; Aboukais, A. Catalytic activity of copper and palladium based catalysts for toluene total oxidation. *Catal. Today* **2007**, *119*, 317–320.
6. Carpentier, J.; Lamonier, J.-F.; Siffert, S.; Zhilinskaya, E.; Aboukais, A. Characterisation of Mg/Al hydrotalcite with interlayer palladium complex for catalytic oxidation of toluene. *Appl. Catal. A* **2002**, *234*, 91–101.
7. Torres, J.Q.; Royer, S.; Bellat, J.-P.; Giraudon, J.-M.; Lamonier, J.-F. Formaldehyde: Catalytic Oxidation as a Promising Soft Way of Elimination. *ChemSusChem* **2013**, *6*, 578–592.
8. Averlant, R.; Royer, S.; Giraudon, J.-M.; Bellat, J.-P.; Bezverkhyy, I.; Weber, G.; Lamonier, J.-F. Mesoporous silica confined MnO_2 nanoparticles as highly efficient catalyst for low temperature elimination of formaldehyde. *ChemCatChem* **2014**, *6*, 152–161.
9. Bai, L.; Wyrwalski, F.; Lamonier, J.-F.; Khodakov, A.Y.; Monflier, E.; Ponchel, A. Effects of β-cyclodextrin introduction to zirconia supported-cobalt oxide catalysts: From molecule-ion associations to complete oxidation of formaldehyde. *Appl. Catal. B* **2013**, *138–139*, 381–390.
10. Torres, J.Q.; Giraudon, J.-M.; Gervasini, A.; Dujardin, C.; Lancelot, C.; Trentesaux, M.; Lamonier, J.-F. Total Oxidation of Formaldehyde over MnO_x–CeO_2 Catalysts: The Effect of Acid Treatment. *ACS Catal.* **2015**, *5*, 2260–2269.
11. Zimowska, M.; Michalik-Zym, A.; Janik, R.; Machej, T.; Gurgul, J.; Socha, R.; Podobinski, J.; Serwicka, E. Catalytic combustion of toluene over mixed Cu–Mn oxides. *Catal. Today* **2007**, *119*, 321–326.

12. Lee, J.; Park, N.; Ryu, S.; Kim, K.; Lee, T. Self-oscillatory behavior in toluene oxidation on zeolite-NaX. *Appl. Catal. A Gen.* **2004**, *275*, 79–86.
13. Ribeiro, M.; Silva, J.; Brimaud, S.; Antunes, A.; Silva, E.; Fernandes, A.; Magnoux, P.; Murphy, D. Improvement of toluene catalytic combustion by addition of cesium in copper exchanged zeolites. *Appl. Catal. B Environ.* **2007**, *70*, 384–392.
14. Weber, G.; Bertrand, O.; Fromont, E.; Bourg, S.; Bouvier, F.; Bissinger, D.; Simmonot-Grange, M.H. TCE Adsorption on Hydrophobic Y and MFI Zeolites. *J. Chim. Phys.* **1996**, *93*, 1412–1425.
15. Fajula, F.; Plee, D. Application of Molecular Sieves in View of Cleaner Technology. *Stud. Surf. Sci. Catal.* **1994**, *85*, 633–651.
16. Benmaamar, Z.; Bengueddach, A. Correlation with different models for adsorption isotherms of m-xylene and toluene on zeolites. *J. Appl. Sci. Environ. Sanit.* **2007**, *2*, 43–56.
17. Jacobs, P.; Linarth, J.; Nijs, H.; Uytterhoeven, J. Redox Behaviour of Transition Metal Ions in Zeolites, Part 5: Method of Quantitative Determination of Bidisperse Distributions of Metal Particle Sizes in Zeolites. *J. Chem. Soc. Faraday Trans.* **1977**, *73*, 1745–1754.
18. Kieger, S.; Delahay, G.; Coq, B. Influence of co-cations in the selective catalytic reduction of NO by NH_3 over copper exchanged faujasite zeolites. *Appl. Catal. B Environ.* **2000**, *25*, 1–9.
19. Torre-Abreu, C.; Henriques, C.; Ribeiro, F.; Delahay, G.; Ribeiro, M. Selective catalytic reduction of NO on copper-exchanged zeolites: The role of the structure of the zeolite in the nature of copper-active sites. *Catal. Today* **1999**, *54*, 407–418.
20. Bulánek, R.; Wichterlová, B.; Sobalík, Z.; Tichý, J. Reducibility and oxidation activity of Cu ions in zeolites: Effect of Cu ion coordination and zeolite framework composition. *Appl. Catal. B Environ.* **2001**, *31*, 13–25.
21. Vijaikumar, S.; Subramanian, T.; Pitchumani, K. Zeolite Encapsulated Nanocrystalline CuO: A Redox Catalyst for the Oxidation of Secondary Alcohols. *J. Nanomater.* **2008**, *2008*, 1–7.
22. Abu-Zied, B. Cu^{2+}-acetate exchanged X zeolites: Preparation, characterization and N_2O decomposition activity. *Microporous Mesoporous Mater.* **2011**, *139*, 59–66.
23. Benaliouche, F.; Boucheffa, Y.; Ayrault, P.; Mignard, S.; Magnoux, P. NH_3-TPD and FTIR spectroscopy of pyridine adsorption studies for characterization of Ag- and Cu-exchanged X zeolites. *Microporous Mesoporous Mater.* **2008**, *111*, 80–88.
24. Dubinin, M.M.; Stoeckli, H.F. Homogeneous and heterogeneous micropore structures in carbonaceous adsorbents. *J. Colloid Interface Sci.* **1980**, *75*, 34–42.
25. Díaz, E.; Ordóñez, S.; Vega, A.; Coca, J. Catalytic combustion of hexane over transition metal modified zeolites NaX and CaA. *Appl. Catal. B Environ.* **2005**, *56*, 313–322.
26. Hammoudi, H.; Bendenia, S.; Marouf-Khelifa, K.; Marouf, R.; Schott, J.; Khelifa, A. Effect of the binary and ternary exchanges on crystallinity and textural properties of X zeolites. *Microporous Mesoporous Mater.* **2008**, *113*, 343–351.
27. Shpiro, E.; Grünert, W.; Joyner, R.; Baeva, G. Nature, distribution and reactivity of copper species in over-exchanged Cu-ZSM-5 catalysts: An XPS/XAES study. *Catal. Lett.* **1994**, *24*,159–169.
28. Ning, P.; Qiu, J.; Wang, X.; Liu, W.; Chen, W. Metal loaded zeolite adsorbents for hydrogen cyanide removal. *J. Environ. Sci.* **2013**, *25*, 808–814.

29. Morales, J.; Sánchez, L.; Martín, F.; Ramos-Barrado, J.; Sánchez, M. Use of low-temperature nanostructured CuO thin films deposited by spray-pyrolysis in lithium cells. *Thin Solid Films* **2005**, *474*, 133–140.
30. Meda, L.; Ranghino, G.; Moretti, G.; Cerofolini, G. XPS detection of some redox phenomena in Cu-zeolites. *Surf. Interface Anal.* **2002**, *33*, 516–521.
31. Gruenert, W.; Sauerlandt, U.; Schloegl, R.; Karge, H. XPS investigations of lanthanum in faujasite-type zeolites. *J. Phys. Chem.* **1993**, *97*, 1413–1419.
32. Almeida, K.; Landers, R.; Cardoso, D. Properties of faujasite zeolites containing methyl-substituted ammonium cations. *J. Catal.* **2012**, *294*, 151–160.
33. Lillo-Ródenas, M.; Cazorla-Amorós, D.; Linares-Solano, A. Behaviour of activated carbons with different pore size distributions and surface oxygen groups for benzene and toluene adsorption at low concentrations. *Carbon* **2005**, *43*, 1758–1767.
34. Archipov, T.; Santra, S.; Ene, A.; Stoll, H.; Rauhut, G.; Roduner, E. Adsorption of Benzene to Copper in CuHY Zeolite. *J. Phys. Chem. C* **2009**, *113*, 4107–4116.
35. Zhang, W.; Qu, Z.; Li, X.; Wang, Y.; Ma, D.; Wu, J. Comparison of dynamic adsorption/desorption characteristics of toluene on different porous materials. *J. Environ. Sci.* **2012**, *24*, 520–528.
36. Boikov, E.; Vishnetskaya, M.; Emel'yanov, A.; Tomskii, I.; Shcherbakov, N. The Selective Catalytic Oxidation of Toluene. *Russ. J. Phys. Chem. A* **2008**, *82*, 2233–2237.
37. Kowenje, C.; Jones, B.; Doetschman, D.; Yang, S.; Kanyi, C. Effects of cation siting and spin-spin interactions on the electron paramagnetic resonance (EPR) of Cu^{2+} exchanged X Faujasite zeolite. *Chem. Phys.* **2006**, *330*, 401–409.
38. Duprat, F. Light-off curve of catalytic reaction and kinetics. *Chem. Eng. Sci.* **2002**, *57*, 901–911.